

Electrocatalytic Activity of $\text{Ni}_x\text{Fe}_{3-x}\text{O}_4$ ($0 \leq x \leq 1.5$) Obtained by Natural Egg Ovalbumin for Alkaline Water Electrolysis

Ritu Yadav¹, Jhasaketan² and N. K. Singh^{1,*}

¹Department of Chemistry, Faculty of Science, University of Lucknow, Lucknow –226007 (India)

²Department of Chemistry, Indian Institute of Technology Kanpur, Kanpur-208016 (India)

*E-mail: nksbhu@yahoo.com; singh_narendra@lkouniv.ac.in

Received: 24 July 2015 / Accepted: 29 August 2015 / Published: 30 September 2015

In the present paper, we reported the synthesis of some Ni-substituted spinel ferrites by low temperature sol-gel method and studied their physicochemical and electrocatalytic properties towards oxygen evolution reaction (OER) in alkaline medium. Nitrate salt of Ni and Fe and freshly extracted egg-white (Ovalbumin) were used as starting materials. X-ray diffraction (XRD) study of the material showed the formation of almost pure spinel phase having some small impurity. For electrochemical studies, materials, so obtained, were transferred in the form of oxide film electrode on Ni-support by oxide slurry painting technique. The voltammogram of each oxide electrode exhibited a pair of redox peaks ($E^\circ = 446 \pm 12$ mV) prior to the OER. The anodic polarization study showed that Ni-substitution in the base oxide increased the electrocatalytic activity considerably and the value was found to be maximum with 0.5 mol Ni ($j = 100$ mA cm⁻² at $E = 865$ mV vs Hg/HgO/ 1M KOH) substitution. Tafel slope values were ranged between 65-102 mV decade⁻¹. Each oxide electrode showed almost first order kinetics with respect to $[\text{OH}^-]$ concentration. The polarization curve has also been recorded at different temperatures in 1 M KOH and with the help of the data obtained at different temperatures, activation energy and other thermodynamic parameters were estimated.

Keywords: Egg white; sol-gel; Spinel-type oxide; Electrocatalysis; Oxygen evolution.

1. INTRODUCTION

Spinel-type oxides of iron are well known technologically important materials for their applications as magnetic recording media, magnetic tapes & fillers, transformer cores, drug delivery, magnetic resonance imaging (MRI) etc. These materials have extensively been used for the decomposition of hydrogen peroxide [1, 2], synthesis of ammonia [3] and oxidation of butene to butadiene [4] in the form of heterogeneous catalysts and as anode materials for synthesis of chlorine and chlorate [5] etc. Various synthetic methods, such as, thermal decomposition [6], freeze-drying [7], citrate precursor techniques [8], co-precipitation [9], sol-gel [10], hydrothermal [11], etc have been

developed to obtain ferrite materials. The conventional ceramic methods require elevated temperatures and prolonged heating time and produce oxides with low specific surface area and limited electrocatalytic performance. Sol-gel [12,13] and co-precipitation [14,15] are found to be well suitable synthetic methods due to their low temperature operation, feasibility and high degree compositional control and produced oxides having relatively high specific surface area vis-à-vis improved catalytic activity. By adopting hydroxide co-precipitation method at a controlled pH (=11), Singh et al. [14, 16-24] synthesized a series of binary and ternary nano-sized spinel ferrites and found considerable enhancement in the electrochemical properties of these materials towards OER. Very recently, we prepared Co-substituted ferrites [25] by citric acid sol-gel route and used them as anode material for oxygen evolution in alkaline medium. In this paper, we used a new synthetic egg-white sol-gel route to produce spinel-type nickel ferrites anode materials for alkaline water electrolysis. The egg-white (ovalbumin) is easily soluble in water and has so many functional properties such as gelling, foaming, emulsification, heat setting and binding adhesion [26]. It has tendency to associate with metal ions such as, $\text{Mn}^{2+}/\text{Mn}^{3+}$, $\text{Fe}^{2+}/\text{Fe}^{3+}$, Cu^{2+} , Zn^{2+} & Ni^{2+} and produces nano-sized materials with interesting properties [27-32]. Results of findings are described in this paper.

2. EXPERIMENTAL

Spinel-type Ni-substituted ferrites used in the present investigation have been synthesized by novel sol-gel method reported in literature [33]. For the purpose, metal salts $\text{Ni}(\text{NO}_3)_2 \cdot 6\text{H}_2\text{O}$ (Merck, 99%), $\text{Fe}(\text{NO}_3)_3 \cdot 9\text{H}_2\text{O}$ (Merck, 98%) were taken in stoichiometric ratio and mixed in the solution of 60 ml freshly extracted egg-white (ovalbumin) and 40 ml of double distilled water. The mixture was vigorously stirred at 27 °C for 2 hrs so as to obtain a well dissolved homogeneous solution. The mixed solution was evaporated on a hot plate at 80 °C with stirring for several hours until a dried precursor was obtained. The dried precursor was crushed into powder using agate pestle mortar and then calcined at 550 °C for 3 hrs to get the desired oxides. Morphology of the sintered oxide powder was examined by scanning electron microscope (SEM; LEO 430). The thermal behaviour of the dried precursor was determined by performing thermo-gravimetric (TG) analysis (Perkin Elmer). IR spectra (Perkin Elmer) of each oxide powder were recorded in the frequency range 4000-400 cm^{-1} . Spinel phase of the catalyst was confirmed by recording powder X-Ray diffraction (XRD) patterns. A Bruker D-8 advanced series-2 diffractometer provided with $\text{Cu-K}\alpha_1$ ($\lambda = 1.54056\text{\AA}$) radiation source was used to record the diffraction pattern.

For electrochemical characterization, the each electrocatalyst was transferred in the form of oxide film electrode on Ni-support ($1.5 \times 1.0 \text{ cm}^2$) by an oxide slurry painting technique [34]. The slurry of the oxide powder with Triton X-100 (Himedia 98%) was coated on one side of the pretreated Ni-support (Aldrich, 99.9%) with help of fine brush and subsequently heat treated at 380 °C for 1½ h. The Ni plate was taken out from the furnace only when the temperature of the furnace becomes below 80 °C so as to get the adherent oxide film. The procedure of the slurry coating was repeated until the desired oxide loading (in mg cm^{-2}) was obtained. The pretreatment of the Ni-support and

electrical contact with the oxide film to form the electrode were performed as described elsewhere [35].

Electrochemical characterizations, such as, cyclic voltammograms (CV) and anodic polarization with regards to OER were carried out in a conventional three electrode single compartment glass cell by using potentiostat/galvanostat (Gamry Reference 600 ZRA) provided with corrosion & physical electrochemistry software and desktop computer (HP). The reference and auxiliary electrodes used in the study were Hg/HgO/1M KOH ($E^\circ = 0.098$ V vs NHE at 25 °C) and pure Pt-foil (area ~ 2 cm²), respectively. All potentials mentioned in the text are measured with respect to the reference Hg/HgO/1M KOH.

3. RESULTS AND DISCUSSION

3.1. Physicochemical Properties

3.1.1. Morphology of oxide powder

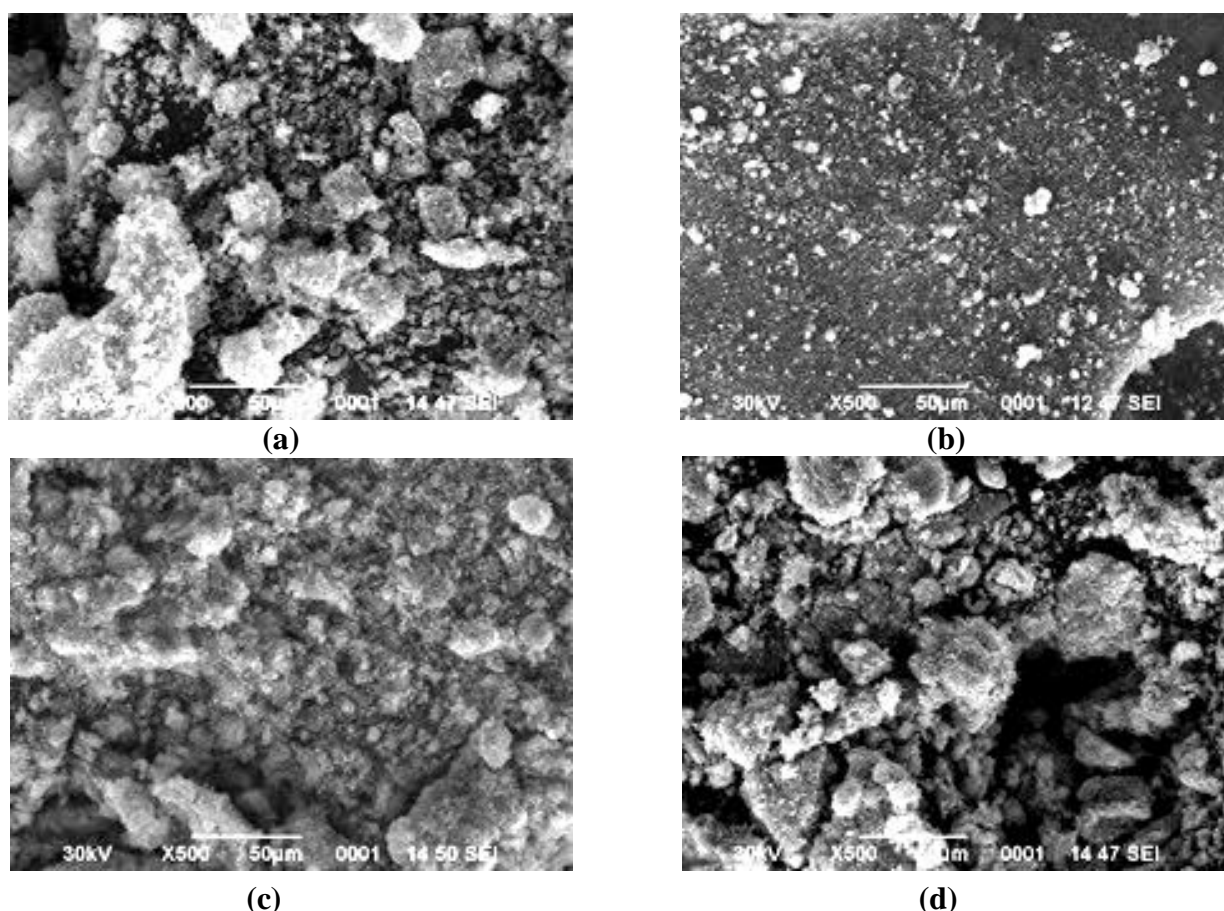


Figure 1. SE micrographs of oxide powders heated at 550 °C for 3 h at magnification ($\times 500$): (a) Fe_3O_4 (b) $\text{Ni}_{0.5}\text{Fe}_{2.5}\text{O}_4$ (c) NiFe_2O_4 (d) $\text{Ni}_{1.5}\text{Fe}_{1.5}\text{O}_4$

The morphology of the oxide powder was examined by scanning electron microscope at different magnifications. SE Micrographs of Fe_3O_4 and its Ni-substituted oxide powder, sintered at 550 °C for 3 hrs, are shown in the Fig.1 (a-d) at the magnification $\times 500$. The figure shows that the

morphology of oxide powder is almost similar. The substitution of the Ni in the base oxide strongly affects the grain size of material except 1.5 mol Ni-substitution. Among the oxides prepare, the morphology of the $\text{Ni}_{0.5}\text{Fe}_{2.5}\text{O}_4$ seemed to be more compact with minimum grain size.

3.1.2. Infrared

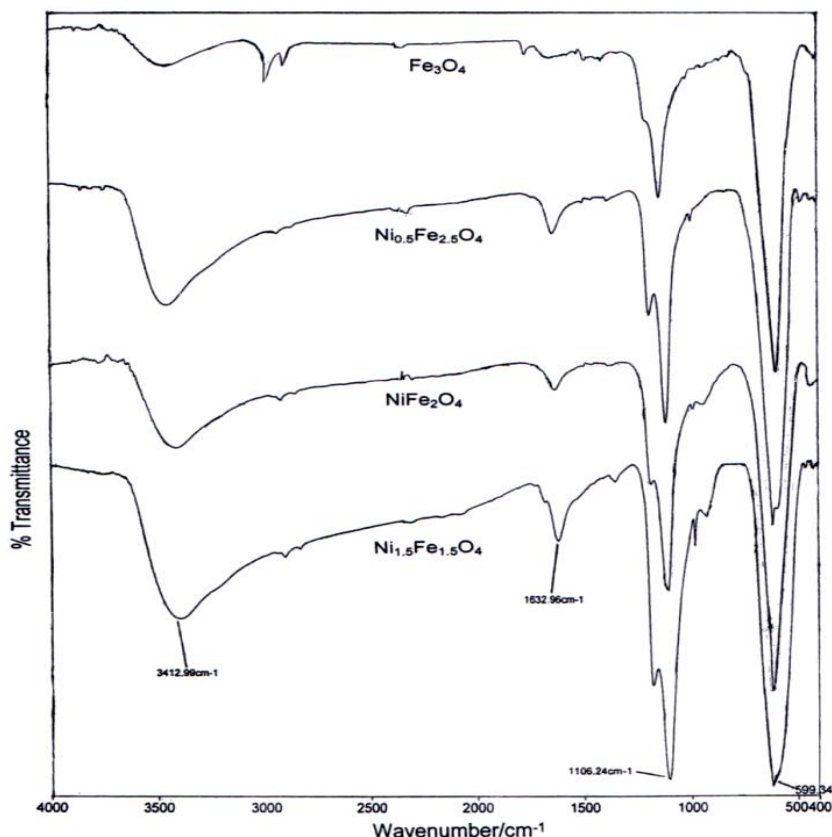


Figure 2. IR spectra of $\text{Ni}_x\text{Fe}_{3-x}\text{O}_4$ ($0 \leq x \leq 1.5$) oxide sintered at 550°C for 3 h.

The IR spectra of each sintered oxide powder (in the form of pellets in KBr), recorded in the region $4000\text{-}400\text{ cm}^{-1}$ (Fig. 2), exhibited a characteristic strong peak at $\sim 599\text{ cm}^{-1}$ of pure spinel ferrite [36, 37]. The observed broad peak at $\sim 3415\text{ cm}^{-1}$ and relatively less intense peak at $\sim 1630\text{ cm}^{-1}$ in the figure corresponds to the O-H stretching vibrations interacting through H-bonds. The peak value at $\sim 1106\text{ cm}^{-1}$ is due to nitrate ion traces.

3.1.3. Thermo-gravimetric (TG) studies

The thermo-gravimetric curve, as shown in the figure 3, indicated total weight loss of 59.6% in the temperature range $30\text{-}550^\circ\text{C}$.

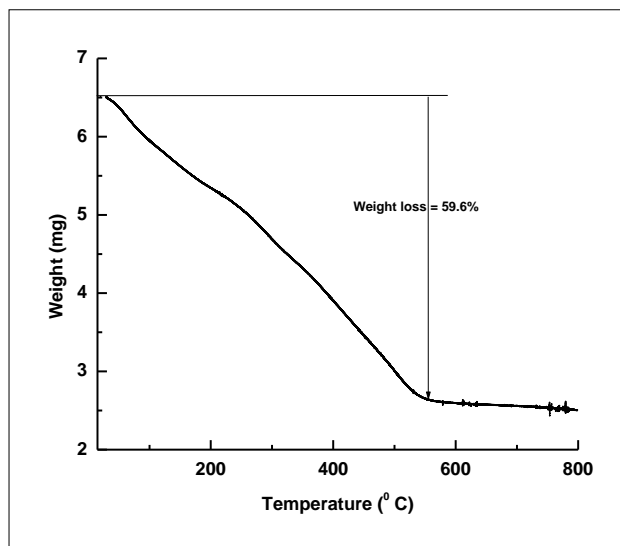


Figure 3. TGA curve dried $\text{Ni}_{0.5}\text{Fe}_{2.5}\text{O}_4$ oxide powder; heating rate $10\text{ }^\circ\text{C}/\text{min}$.

The corresponding weight loss is due to the evaporation of moisture, solvent and combustion of organic ovalbumin matrix present in oxide precursor.

3.1.4. X-Ray Diffraction (XRD)

Powder X-ray diffraction pattern of each catalyst was recorded between $2\theta = 20^\circ$ and $2\theta = 70^\circ$. The diffraction pattern of the oxide Fe_3O_4 and NiFe_2O_4 is shown in Fig. 4.

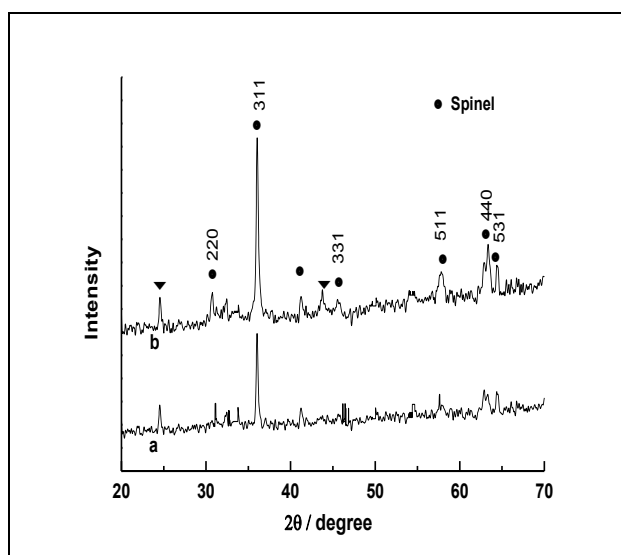


Figure 4. X-ray diffraction pattern of $\text{Ni}_x\text{Fe}_{3-x}\text{O}_4$, sintered at 550°C for 3 h; (a) $x = 0$ mol (b) $x = 1.0$ mol

From figure it is observed that the diffraction of the oxide are more closely packed with the literature JCPDS-ASTM files 02-1035 and 10-0325 reported for Fe_3O_4 and NiFe_2O_4 , respectively.

However, the presence of some additional peaks corresponding to d -values 1.69, 1.84, 2.69 and 3.68 Å in the figure indicate the existence of Fe_2O_3 (JCPDS-ASTM file 01-1053) in the oxide lattice. The most intense diffraction peak (311) of the pattern for a particular oxide is taken to determine the crystallite size of the oxide by using the Scherer's formula [38] and values, so obtained were 32 and 26 nm for Fe_3O_4 and NiFe_2O_4 , respectively.

3.2. Electrochemical properties

3.2.1. Cyclic Voltammetry (CV)

Cyclic voltammogram of each oxide film electrode was recorded in the potential region 0.0-0.7 V in 1M KOH at 25 °C. Fig. 5 shows the CV curve of oxide Electrocatalysts at the scan rate of 20 mV sec^{-1} .

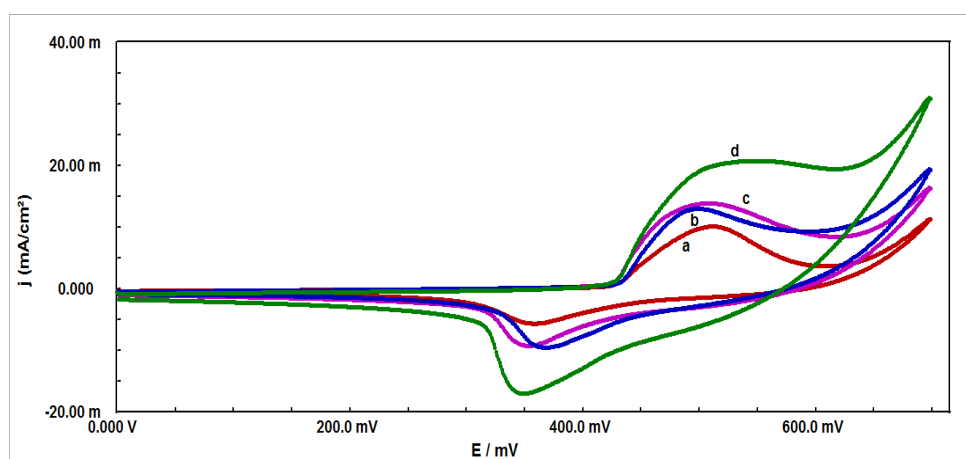


Figure 5. Cyclic Voltammogram of oxide film electrodes on a Ni-substrate at 20 mV s^{-1} in 1 M KOH at 25 °C; (a) Fe_3O_4 , (b) $\text{Ni}_{1.5}\text{Fe}_{1.5}\text{O}_4$, (c) NiFe_2O_4 and (d) $\text{Ni}_{0.5}\text{Fe}_{2.5}\text{O}_4$

From figure, it is clear that each oxide exhibited a pair of redox peak (anodic and corresponding cathodic) prior to the onset of oxygen evolution reaction. Values of anodic (E_{pa}) and cathodic (E_{pc}) peak potentials, the peak separation potential ($\Delta E_p = E_{pa} - E_{pc}$) and the formal redox potential [$E^\circ = (E_{pa} + E_{pc})/2$] have been estimated from the CV curves and listed in the Table 1. The table 1 shows that the substitution of Ni in the base oxide slightly increased the ΔE values whereas formal redox potential (E°) values were found to be almost similar with each introduction of Ni. In order to know the origin of the redox peaks, electrodes of the similar oxides on Pt-substrate have been prepared and recorded the cyclic voltammogram by keeping all experimental conditions similar. The absence of redox peaks in the cyclic voltammetric curve of the oxide electrode on Pt indicates that the observed redox peaks were originated from the Ni-support through the electrolyte contact and not to the oxidation of nickel ferrite film surface [14]. It is reported [14, 39] that the oxides prepared at low temperature undergo hydration in the electrolytic solution which comes in contact with the Ni-substrate through pores and grain boundaries.

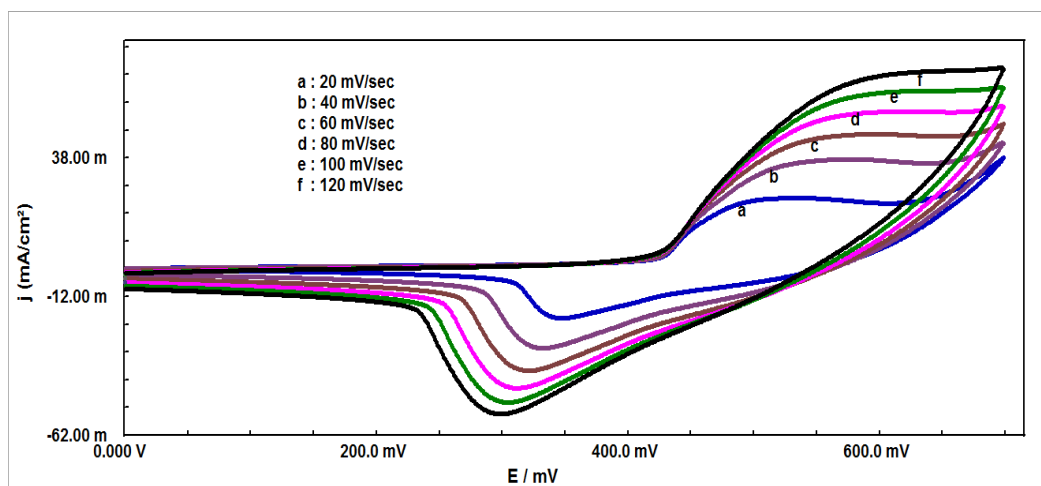


Figure 6. Cyclic voltammogram of the Ni/Ni_{0.5}Fe_{2.5}O₄ electrode at different scan rates in 1 M KOH (25 °C).

The effect of scan rates on the peak separation potential has also been studied. For the purpose, scan rates 20 to 120 mV s⁻¹ were used to run the cyclic voltammogram (Fig. 6) and found that both anodic and cathodic peaks became further apart with increase in scan rate. It was observed that with six fold increase in the scan rate, the ΔE_p values shifted from 133 – 253, 187 – 368, 210 – 305 and 131 – 235 for the oxide electrodes Fe₃O₄, Ni_{0.5}Fe_{2.5}O₄, NiFe₂O₄ and Ni_{1.5}Fe_{1.5}O₄, respectively. The voltammetric charge (q) was estimated by integrating the CV curve from zero to a potential just prior to the start of oxygen evolution [40]. The plot of q vs (scan rate)^{-1/2} was found to be linear which indicates that the surface redox reaction is diffusion controlled [40].

Table 1. Results of the cyclic voltammetric parameters on Ni/Ni_xFe_{3-x}O₄ (0 ≤ x ≤ 1.5) in 1 M KOH at 25 °C at the scan rate 20 mV s⁻¹.

Oxide Electrode	E _{pa} / mV	E _{pc} / mV	$\Delta E = (E_{pa} - E_{pc})$ / mV	E° = (E _{pa} + E _{pc})/2 / mV
Fe ₃ O ₄	505	362	143	434
Ni _{0.5} Fe _{2.5} O ₄	542	349	193	445
NiFe ₂ O ₄	539	356	183	448
Ni _{1.5} Fe _{1.5} O ₄	548	365	183	457

3.2.2. Electrocatalytic activity

The electrocatalytic activity of the spinel oxide electrodes was determined by recording the iR -uncompensated anodic polarization curve (E vs $\log j$) at potential scan rate of 0.2 mV s⁻¹ in 1 M KOH at 25 °C. The polarization curve of each oxide electrode is shown in Fig. 7.

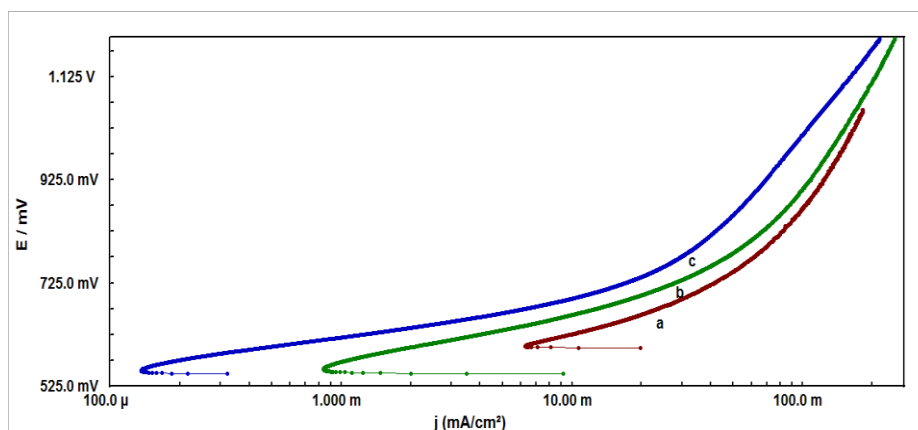


Figure 7. Anodic polarization curve for oxygen evolution reaction on the $\text{Ni/Ni}_x\text{Fe}_{3-x}\text{O}_4$ ($0 \leq x \leq 1.5$) electrode in 1 M KOH at 25 °C (scan rate = 0.2 mV s^{-1}). (a) $\text{Ni}_{0.5}\text{Fe}_{2.5}\text{O}_4$ (b) NiFe_2O_4 and (c) Fe_3O_4

All curves obtained were similar in nature and have one Tafel slope in low potential region. A very high Tafel slope was observed in the higher potential region. This might be due to the polarization of the curve with increasing applied potential. Values of Tafel slope and electrocatalytic activity in terms of current density at three different potentials as well as in terms of potential at fixed current density were estimated from the polarization curve and shown in the Table 2. Values of Tafel slope were ranged between $65\text{-}102 \text{ mV decade}^{-1}$. The observed b-value with Fe_3O_4 electrode was found to be very close to $2.3RT/F$. However, Ni-substitution in the base oxides exhibited higher Tafel slope value which is close to $3 \times 2.3RT/2F$ for oxygen evolution reaction. The substitution of Ni in the base oxide also increased the electrocatalytic activity and the value was found to be maximum with 0.5 mol Ni-substitution.

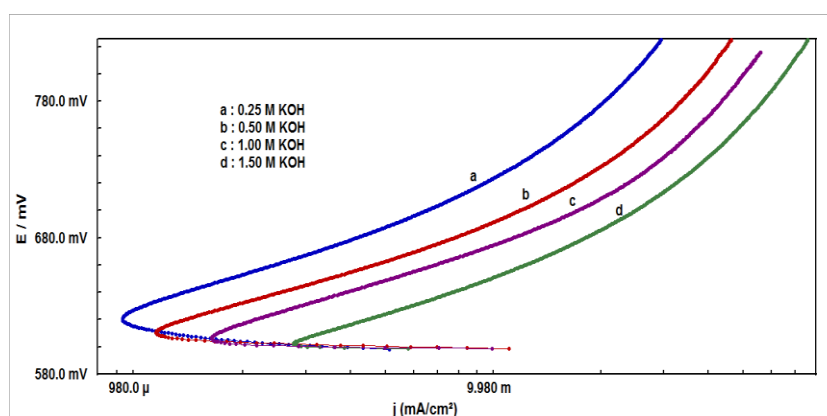


Figure 8. Anodic polarization curve for oxygen evolution on $\text{Ni/Ni}_{0.5}\text{Fe}_{2.5}\text{O}_4$ electrode at varying KOH concentrations ($\mu = 1.5$) at 25 °C.

The catalytic activity of the 0.5 mol Ni-substituted oxide was observed to be ~ 4 times (at 650 mV) higher than that of base oxide. Based on the apparent current density data at a certain potential ($E = 850 \text{ mV}$) the electrocatalytic activity of oxides followed the order:

$\text{Ni}_{0.5}\text{Fe}_{2.5}\text{O}_4$ ($j_a = 108.8 \text{ mA cm}^{-2}$) > NiFe_2O_4 ($j_a = 82.5 \text{ mA cm}^{-2}$) > $\text{Ni}_{1.5}\text{Fe}_{1.5}\text{O}_4$ ($j_a = 71.8 \text{ mA cm}^{-2}$) > Fe_3O_4 ($j_a = 59.6 \text{ mA cm}^{-2}$)

The reaction order (p) with respect to OH^- concentration, for oxygen evolution reaction, was determined by recording the anodic polarization curve (Fig. 8) in different KOH concentrations.

The ionic strength of the electrolyte was kept constant ($\mu = 1.5$) by using KNO_3 (Merck 98%) as an inert electrolyte. The value of reaction order estimated from the slope of the plot $\log j$ vs $\log [\text{OH}^-]$ (Fig. 9) at a fixed potential ($E = 650 \text{ mV}$) was found to be unity with each oxide electrode.

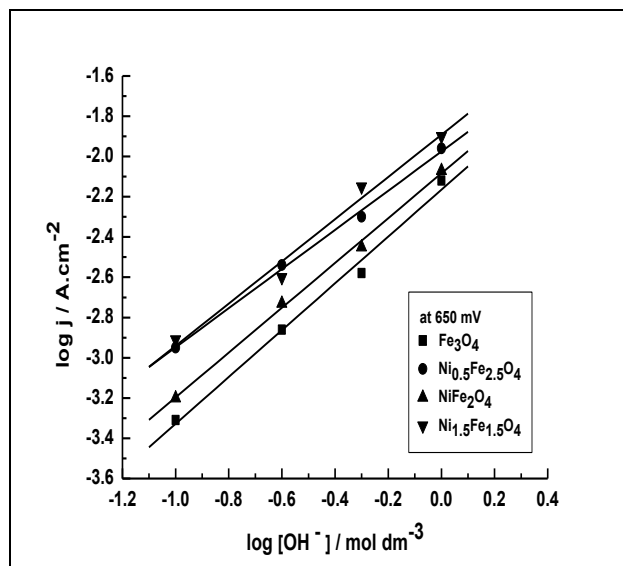


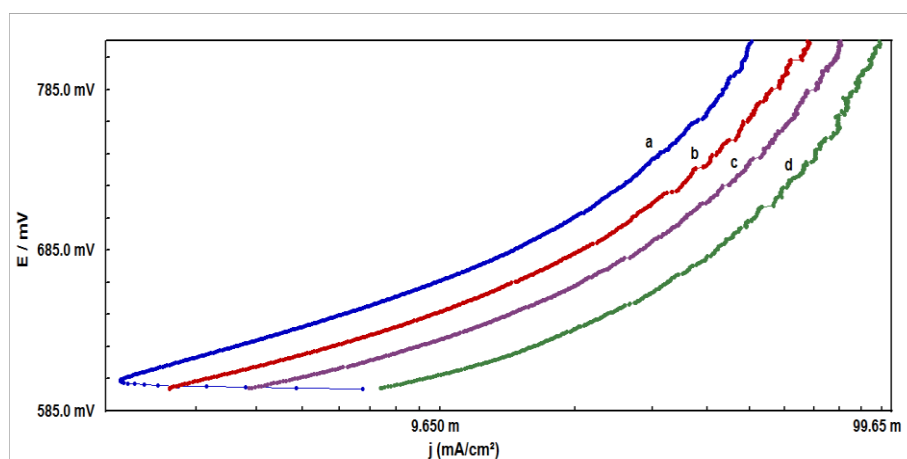
Figure 9. Plot of $\log j$ vs $\log C_{\text{OH}^-}$ of the oxide electrodes at a constant potential ($E = 650 \text{ mV}$) across the oxide/1 M KOH interface at 25°C .

Generally, current density values of the first Tafel region of the polarization curve, obtained at different KOH concentrations were chosen for the determination of order of reaction. The observed values of reaction order and Tafel slope suggest that pure and Ni-substituted ferrite follow two different mechanistic paths. The Tafel slope observed by us was almost similar to that observed Singh et al. [18] for the case of Cu-substituted ferrites ($75\text{--}110 \text{ mV decade}^{-1}$) prepared by hydroxide coprecipitation method. However, it is remarkable that the electrocatalytic activity of the oxide electrodes in the present study was found to be higher than those reported by Orehtsky et al. [7] ($j = 10 \text{ mA cm}^{-2}$ at $\eta_{\text{O}_2} = 0.34 \text{ V}$ for NiFe_2O_4 in 30 wt% KOH), Singh et al. [18] ($j = 1.2\text{--}7.2 \text{ mA cm}^{-2}$ at $E = 0.7 \text{ V}$ in 1 M KOH at 25°C particularly for Cu-substituted ferrites) and Al-Mayouf et al. [41] ($j = 0.62 \text{ mA cm}^{-2}$ at $E = 0.65 \text{ V}$ in 1M KOH at 25°C for NiFe_2O_4 prepared by hydrothermal method). The oxide electrode, $\text{Ni}_{0.5}\text{Fe}_{2.5}\text{O}_4$, obtained by this method ($j = 19.6 \text{ mA cm}^{-2}$ at $E = 0.65 \text{ V}$) is ~ 7 times more active than $\text{Co}_{0.5}\text{Fe}_{2.5}\text{O}_4$ ($j = 2.7 \text{ mA cm}^{-2}$ at $E = 0.65 \text{ V}$) obtained by citric acid sol-gel route [25]. The η_{O_2} is the formal overpotential; $\eta_{\text{O}_2} = E - E_{\text{O}_2/\text{OH}^-}$, where E and $E_{\text{O}_2/\text{OH}^-}$ ($= 0.303 \text{ V vs Hg/HgO}$) are the applied potential across the catalysts/1 M KOH interface and the theoretical equilibrium potential in 1 M KOH at 25°C .

Table 2. Values of electrode kinetic parameter for O₂ evolution on Ni/Ni_xFe_{3-x}O₄ (0 ≤ x ≤ 1.5) 1 M KOH at 25 °C (scan rate = 0.2 mV s⁻¹).

Electrodes	Tafel slope (<i>b</i>) (mV decade ⁻¹)	Order (<i>p</i>)	<i>E</i> /mV at <i>j</i> (mA cm ⁻²)		<i>j</i> (mA cm ⁻²) at <i>E</i> / mV		
			10	100	650	750	850
Fe ₃ O ₄	65	1.1	677	963	4.9	29.8	59.6
Ni _{0.5} Fe _{2.5} O ₄	102	1.0	624	865	19.6	60.0	108.8
NiFe ₂ O ₄	82	1.0	661	888	7.9	40.0	82.5
Ni _{1.5} Fe _{1.5} O ₄	90	1.1	658	917	10.2	36.3	71.8

The temperature variation effect of the oxide electrocatalyst on the OER has been studied by recording the anodic polarization curves at different temperature in 1 M KOH. A representative Tafel plot for Ni_{0.5}Fe_{2.5}O₄ is shown in Fig. 10.

**Figure 10.** Anodic polarization curve for Ni/Ni_{0.5}Fe_{2.5}O₄ electrode in 1 M KOH at different temperatures (scan rate = 0.2 mV s⁻¹) (a) 20 °C, (b) 30 °C, (c) 40 °C and (d) 50 °C

Form the data of the polarization curve, a graph $\log j$ vs $1/T$ was plotted at different potential which is shown in the Fig. 11. Slope of the plot gives the value of standard apparent enthalpy of activation ($\Delta H_{el}^{\circ\#}$). Figure 11 showed that the value of $\Delta H_{el}^{\circ\#}$ decreases with the increase of applied potential. It has been observed that the value of $\Delta H_{el}^{\circ\#}$ is almost similar to that reported on Adams-RuO₂ (49 kJ mol⁻¹) [42], oxide coated Co₅₀Ni₂₅Si₁₅B₁₀ amorphous alloy (40 kJ mol⁻¹) [43] and Cu_{0.9}Co_{2.1}O₄ (45.2 kJ mol⁻¹) [44].

The transfer coefficient (α) is estimated from the equation $\alpha = 2.303RT/bF$, where '*b*' is the Tafel slope obtained from the polarization curves recorded at different temperatures. *F* and *R* are the Faraday constant and gas constant, respectively. The relation, $\Delta H_{el}^{\circ\#} = \Delta H^{\circ\#} - \alpha F \eta$ was used to estimate the standard enthalpy of activation ($\Delta H^{\circ\#}$) or standard electrochemical enthalpy of activation. The standard entropy of activation ($\Delta S^{\circ\#}$) was calculated by using the relation [16, 45]:

$$\Delta S^{\circ\#} = 2.3R [\log j + \Delta H_{el}^{\circ\#} / 2.3RT - \log (nF\omega C_{OH^-})]$$

Where, *n* (= 2) is the number of electron transfer for OER in alkaline medium. ω ($= k_B T/h$) is the frequency term. C_{OH^-} is the electrolyte concentration and *j* is the current density at a certain

potential. The estimated values of transfer coefficient (α), and all other thermodynamic parameters are given in Table 3. The data shown in Table 3 indicates that Ni-substitution in the base oxide decreased the $\Delta H^{\circ\#}$ value. Values of standard entropy of activation ($\Delta S^{\circ\#}$) for oxygen evolution were found to be highly negative. This suggests the role of adsorption phenomenon in the electrochemical formation of oxygen [16, 25].

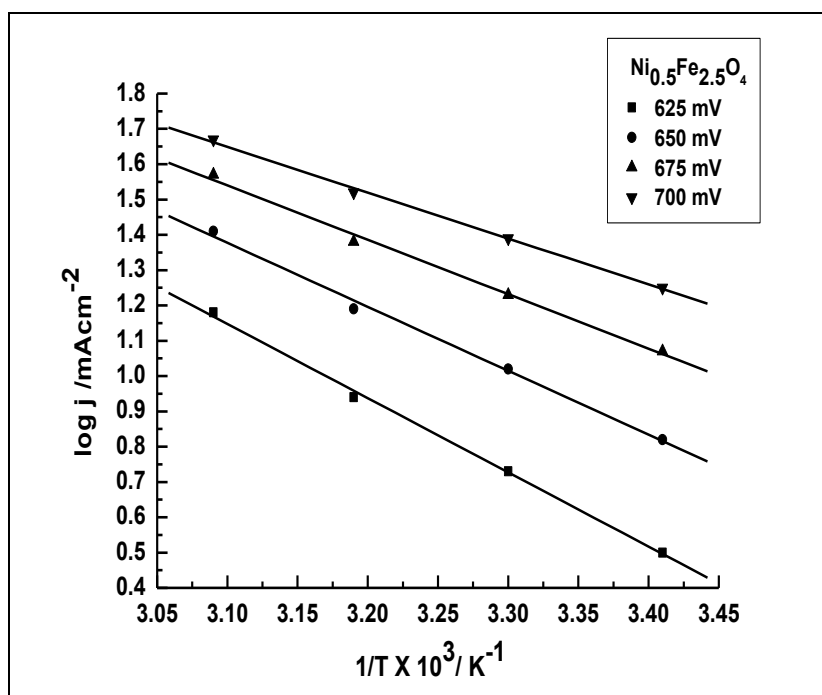


Figure 11. Arrhenius plot for oxygen evolution reaction on Ni/Ni_{0.5}Fe_{2.5}O₄ at different potential.

Table 3. Values of thermodynamic parameters for O₂ evolution on Ni/Ni_xFe_{3-x}O₄ (0 ≤ x ≤ 1.5) 1M KOH

Electrode	$\Delta H_{el}^{\circ\#}$ (kJ mol ⁻¹) at (E = 625 mV)	$-\Delta S^{\circ\#}$ (J deg ⁻¹ mol ⁻¹)	α	$\Delta H^{\circ\#}$ (kJ mol ⁻¹)
Fe ₃ O ₄	45.9	185.5	0.9	63.5
Ni _{0.5} Fe _{2.5} O ₄	38.4	197.2	0.6	56.4
NiFe ₂ O ₄	42.7	150.0	0.9	62.7

4. CONCLUSION

The study shows that Ni substitution in the base oxide for Fe enhances the electrocatalytic activity of the oxide toward the OER. The catalytic activity of the most active electrode (Ni_{0.5}Fe_{2.5}O₄) was found to be about four times higher than the base oxide at 650 mV. Thermodynamic parameters of the oxide electrode were also affected by the Ni-substitution.

ACKNOWLEDGEMENTS

Authors are thankful to Department of Science and Technology (DST), New Delhi for financial support as Fast Track Scheme for Young Scientist (No.: SR/FT/CS-044/2009).

References

1. P. Lahari, S. K. Sengupta, *J. Chem. Soc. Faraday Trans.* 91 (1995) 3489-3494.
2. H. M. Kota, J. Katan, M. Chin, F. J. Schoenweis, *Nature* 203 (1964) 1281.
3. R. R. Rajaram, P. A. Sermon *J. Chem. Soc. Faraday Trans.* 81 (1985) 2577-2591.
4. H. K. Harold, C. K. Mayfair, *Adv. Catal.* 33 (1985) 159-198.
5. S. Trasatti, G. Lodi (1981) In: S. Trasatti (ed) *Electrodes of conductive metallic oxides*, part B, Elsevier, Amsterdam, pp 521-625.
6. C. Iwakura, M. Nishioka, H. Tamura, *Nippon Kagaku Kaishi* 7 (1982) 1136-1140.
7. J. Orehotsky, H. Huang, C.R. Davidson, S. Srinivasan, *J. Electroanal. Chem.* 95 (1979) 233-235.
8. S. Prasad, N. S. Gajbhiye, *J. Alloys Compd.* 265 (1998) 87-92.
9. J. M. Yang, W. J. Tsuo, F. S. Yen, *J. Solid State Chem.* 145 (1999) 50-57.
10. D. H. Chen, X. R. He, *Mater Res Bull* 26 (2001) 1369-1377.
11. J. Zhou, J. Ma, C. Sun, L. Xie, Z. Zhao, H. Tian, *J. Am. Ceram. Soc.* 88 (2005) 3535-3537.
12. M. El Baydi, G. Poillerat, J. L. Rehspringer, J. L. Gautier, J. F. Koenig and P. Chartier, *J. Solid State Chem.* 109 (1994) 281-288.
13. J. L. Martin de Vidales, O. Garcia Martinez, E. Vila, R. M. Rojas, M. J. Torralvo, *Mat Res. Bull.* 28 (1993) 1135-1143.
14. N. K. Singh, S. K. Tiwari, K. L. Anitha, R. N. Singh, *J. Chem. Soc. Faraday Trans.* 92(13) (1996) 2397-2400.
15. Guo-Hui Li, Li-Zhem Dai, Da-Shun Lu and Shao-Yi Peng, *J. Solid State Chemistry*, 89 (1990) 167-173.
16. R. N. Singh, N. K. Singh, J. P. Singh, *Electrochim. Acta* 47 (2002) 3873-3879.
17. R. N. Singh, N. K. Singh, J. P. Singh, G. Balaji, N. S. Gajbhiye, *Int. J. Hydrogen Energy* 31 (2006) 701-707.
18. J. P. Singh, N. K. Singh, R. N. Singh, *Int. J. Hydrogen Energy* 24 (1999) 433-439.
19. R. N. Singh, J. P. Singh, B. Lal, A. Singh, *Int. J. Hydrogen Energy* 32 (2007) 11-16.
20. N. K. Singh, R. N. Singh, *Ind. J. Chem.* 38A (1999) 491-495.
21. R. N. Singh, J. P. Singh, A. Singh, *Int. J. Hydrogen Energy* 33 (2008) 4260-4264.
22. R. N. Singh, J. P. Singh, B. Lal, M. J. K. Thomas, S. Bera, *Electrochim. Acta* 51 (2006) 5515-5523.
23. R. N. Singh, J. P. Singh, H. N. Cong, P. Chartier, *Int. J. Hydrogen Energy* 31 (2006) 1372-1378.
24. Anindita, A. Singh, R. N. Singh, *Int. J. Hydrogen Energy* 35 (2010) 3243-3248.
25. Ritu Yadav, M. K. Yadav, N. K. Singh, *Int. J. Electrochem. Sci.* 8 (2013) 6321-6331.
26. Y. Mine, *Worlds Poult Sci J.* 58 (2002) 31-39.
27. M. A. Gabal, *Mater Lett.* 64(17) (2010) 1887-1890.
28. S. M. Senthil, R. Jayaprakash, V. N. Singh, B. R. Mehta, G. Govindaraj, *Nano Res.* 4 (2008) 107-116.
29. S. M. Senthil, R. Jayaprakash, S. R. Murthy, A. R. Phani, V. N. Singh, G. Govindaraj, *Nano Res.* 6 (2009) 205-213.
30. Z. Durmus, A. Baykal, H. Kavas, M. Direkçi, M. S. Toprak, *Polyhedron* 28(11) (2009) 2119-2122.
31. F. Nouroozi, F. Farzaneh, *J. Braz Chem. Soc.* 22(3) (2011) 484-488.
32. S. Maensiri, C. Masingboon, P. Laokul, et al. *Cryst Growth Des.* 7(5) (2007) 950-955.
33. S. Maensiri, C. Masingboon, B. Boonchom, S. Seraphin, *Scripta Materialia* 56 (2007) 797-800.
34. S. K. Tiwari, P. Chartier, R. N. Singh, *J. Electrochem. Soc.* 142(1) (1995) 148-153.
35. R. N. Singh, J. F. Koenig, G. Poillerat, P. Chartier, *J Electrochem. Soc.* 137 (1990) 1408-1413.

36. B. Gillot, M. Laarj, S. Kacim, *J. Mater. Chem.* 7 (1997) 827-831.
37. B. Gillot, V. Nivoix, E. Kester, O. Nusillard, C. Villette, Ph. Tailhades, A. Rousset, *Mater. Chem. Phys.* 48 (1997) 111-118.
38. N. Fradette, B. Marsan, *J. Electrochem. Soc.*, 145 (1998) 2320-2327.
39. C. Iwakura, A. Honji, H. Tamura, *Electrochim. Acta* 26 (1981) 1319-1326.
40. R. N. Singh, S. K. Tiwari, S. P. Singh, N. K. Singh, G. Poillerat, P. Chartier, *J. Chem. Soc. Faraday Trans.* 92(14) (1996) 2593-2598.
41. M.S. AL-Hoshan, J. P. Singh, A. M. Al-Mayouf, A. A. Al-suhybani and M. N. Shaddad, *Int. J. Electrochem. Sci.*, 7 (2012) 4959-4973.
42. A. Mills, H. L. Davis, *Electrochim. Acta* 37(7) (1992) 1217-1225.
43. T. Kessler, W. E. Triaca, A. J. Arvia, *J. Appl. Electrochem.*, 24 (1994) 310-315.
44. I. Nikolov, R. Darkaou, E. Zhecheva, R. Stoyanova, N. Dimitrov, T. Vitanov, *J. Electroanal. Chem.* 429 (1997) 157-168.
45. E. Gileadi, *Electrode Kinetics*, VCH Publishers Inc., New York, 1993, p. 151.

© 2015 The Authors. Published by ESG (www.electrochemsci.org). This article is an open access article distributed under the terms and conditions of the Creative Commons Attribution license (<http://creativecommons.org/licenses/by/4.0/>).